Kosterlitz - Thouless behaviour in $Tl_2Ba_2CaCu_2O_8$ granular thin films

1996 J. Phys.: Condens. Matter 8 11193

(http://iopscience.iop.org/0953-8984/8/50/041)

J. Phys.: Condens. Matter **8** (1996) 11193–11204. Printed in the UK

Kosterlitz–Thouless behaviour in $Tl_2Ba_2CaCu_2O_8$ granular thin films

J C Soret†, L Ammor†, A Smina†, B Martinie†, A Ruyter†, J Lecomte†, Ch Gasser‡, Ch Goupil‡ and Ch Simon‡

† Laboratoire de Physique Electronique et Thermodynamique des Oxydes, Université de Tours, Unité de Formations et de Recherches Sciences et Techniques, 37200 Tours, France

‡ Laboratoire de Cristallographie et Sciences des Matériaux Unité de Recherche associée au CNRS 1318, Institut des Sciences de la Matière et du Rayonnement, 14050 Caen Cédex, France

Received 12 July 1996, in final form 12 September 1996

Abstract. Current–voltage characteristics are reported for a $Tl_2Ba_2CaCu_2O_8$ thin film with a granular structure. Our data provide support for a Berezinskii–Kosterlitz–Thouless transition type with an unusual vortex–antivortex interaction $A(T) \sim (T_{co} - T)^2$. Dissipation is discussed in terms of large-scale pair excitations through the sample inhomogeneities. Consistency is found with the theory worked out by Lobb, Abraham and Tinkham to explain resistive transition data in arrays of superconducting junctions arranged two-dimensionally. On this basis, the temperature behaviour of $A(T)$ accounts for a weakening of the pair potential at interfaces due to the short coherence length of high-T_c oxides, as was pointed out by Deutscher and Müller. We investigate the spatial renormalization of the vortex–antivortex interaction over the length scale probed by the current in the same manner as was first demonstrated by Kadin, Epstein and Goldman. Then good agreement with the renormalized Kosterlitz–Thouless theory is found.

1. Introduction

Voltage–current (V–I) characteristics of high-T_c superconductors in a zero magnetic field have been reported extensively to exhibit a power-law behaviour $V \sim I^a$ with an exponent $a > 3$ depending on the temperature, below a characteristic temperature above which a non-zero ohmic resistance is observed [1–10]. Usually, the origin of this non-ohmic regime has been interpreted as resulting from the quasi-two-dimensional (2D) superconducting-like behaviour of the cuprate superconductors. In this approach, the dissipation has been explained on the basis of the Berezinskii–Kosterlitz–Thouless (BKT) [11, 12] phase transition theory [13] of non-binding vortex pair excitations within the superconducting CuO_2 layers. In this way, similarly to layered spin systems with planar rotator symmetry [14], oxide cuprate superconductors appear as 2D X–Y-like systems except in a narrow region near the BKT critical temperature T_{BKT}, which reflects the finite anisotropy of the material [3, 5–8, 15]. Another possible approach, which should be more appropriate for a description of the resistive transition in granular thin films, refers to the theory worked out by Lobb, Abraham and Tinkham (LAT) [16] to explain resistive transition data in arrays of superconducting junctions arranged two-dimensionally many years ago.

In both approaches as proposed above, two types of 2D vortex–antivortex pair excitation are considered, respectively. One concerns the phase fluctuations within the individual superconducting CuO_2 layers in which the space scale is determined by the in-plane coherence length $\xi_\parallel$, and the other is large-scale phase fluctuations through sample

0953-8984/96/5011193+12$19.50

inhomogeneities. Here, one can wonder whether it is possible to make a distinction between these two types of vortex–antivortex pair excitation or not from the experiment. As will be shown below, the latter are essential to explain the electrical properties in some granular thin films in high-T_c materials in which the grain size s is much greater than the in-plane coherence length, namely $s \gg \xi_\parallel$. In both these cases, vortices and antivortices show the same logarithmic interaction $U(r) = 2\pi\kappa_0 k_B T \ln(r/r_0) + 2\mu_c$, where $2\mu_c$ is the energy required to create a pair at the smallest separation possible r_0 which is determined by either $\xi_\parallel$ or s. The stiffness constant $\pi\kappa_0$ affecting the vortex interaction constant $A = 2\pi\kappa_0 k_B T$ depends on the nature of vortices and usually varies as a function of the temperature, vanishing at the mean-field temperature T_{co}. In 2D arrays of superconductor–insulator–superconductor (SIS) tunnel junctions and in high-T_c materials, the vortex interaction will have near T_{co} an anomalous temperature dependence $A(T) \sim (T_{co} - T)^2$ [17]. This results from the fact that SIS junctions show, similarly to the so-called proximity effect for superconductor–normal–superconductor (SNS) tunnel junctions [18], a strongly depressed order parameter at the interface, near T_{co} because high-T_c oxides have extremely short coherence lengths [19, 20]. Consequently, one expects for both SIS and SNS tunnel junction arrays the same temperature dependence for A, namely $A(T) \sim (T_{co} - T)^2$. Note that this temperature behaviour cannot account for 2D vortex pair excitations within the superconducting CuO_2 layers. This is because the in-plane vortex–antivortex interaction is predicted, in the zero Josephson interlayer coupling limit, to be proportional to the sheet density of Cooper pairs: $n^*_{2D} = n^*_{3D} d \sim (T_{co} - T)$, where d is the efective thickness of superconducting layers [21–23]. Nevertheless, irrespective of any temperature dependence for A, the renormalization of the vortex interaction yields a theoretical universal scaling behaviour for the BKT phase transition whose experimental investigation is, in principle, a way of probing the vortex interaction. In particular, taking into account the finite current effects on the BKT behaviour, Kadin, Epstein and Goldman (KEG) [24] have shown that the current dependence of the curvature of V–I curves, near T_{BKT}, is a direct measure of the partially renormalized stiffness constant $\kappa_{\ell_I}(T)$ over characteristic distances $\xi_I = r_0(I_c/I)$ with the corresponding dimensionless quantity $\ell_I = \ln(\xi_I/r_0)$ for which the characteristic current I_c is proportional to the vortex interaction constant A.

The present paper reports the electrical transport properties of a c-axis-oriented $Tl_2Ba_2CaCu_2O_8$ (Tl-2212) thin film with granular structure. The data are analysed within the framework of the LAT model [16]. From isothermal I–V curves we have been able to investigate the spatial renormalization of the vortex–antivortex interaction. Section 2 is concerned with the experimental method. The experimental results are presented in section 3; in particular, an unusual method is proposed to determine the vortex interaction constant. In section 4, we discuss the current-dependent curvature of I–V characteristics on the basis of the renormalized Kosterlitz–Thouless phase transition theory.

2. Experimental method

The Tl-2212 thin film with a thickness of 500 nm was deposited on an oriented $LaAlO_3(100)$ substrate from a multitarget sputtering process as was described elsewhere [25]. The annealing process was performed according to the method used for the synthesis in sealed quartz tube [26]. Before starting the annealing cycle, the film was wrapped in a gold foil in the presence of a Tl-2212 pellet in order to introduce a thallium oxide pressure [27] and placed with a crucible containing a mixture of Tl_2O_3 and BaO_2 in a quartz tube which was sealed after pumping in air to 10^{-2} mbar. The tube was heated at a rate of $8.5\,^\circ$C min^{-1} up to $870\,^\circ$C for 10 min, and afterwards the furnace was cooled to room temperature. Owing

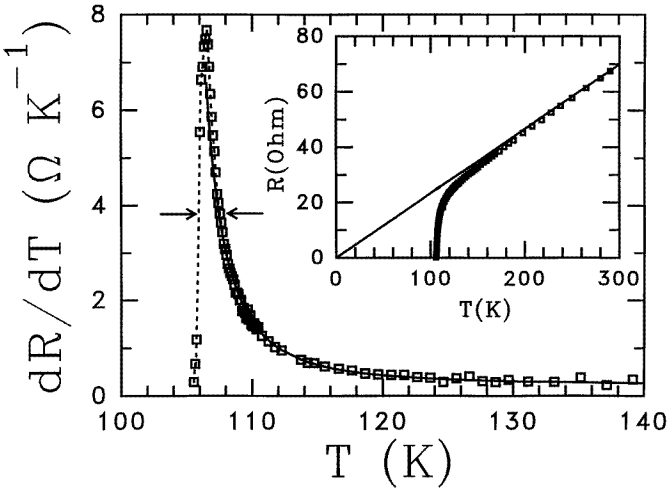

Figure 1. Derivative of R with respect to T versus T. The broken line is a guide for the eyes and the solid curve displays an attempt to fit equation (6) to the data. The two antiparallel arrows give an estimate for the broadening of the resistive transition. The inset shows R versus T. The straight line exhibits a linear fit to the high-temperature data.

to the mixed Tl_2O_3 and BaO_2, an oxygen partial pressure of about 10 mbar was expected during the dwell time. Using this annealing process, high-quality films were obtained as was proved by transmission electron miscroscopy [26]. The electron diffraction patterns exhibited sharp reflections; the cell parameters and the space group were typical of a 2212-type structure. Moreover, the corresponding bright-field images showed good periodicity of the layer stacking along the c axis in agreement with the sharp reflections. Scanning electron micrographs revealed homogeneous crystallization.

Two bridges with corresponding four-point measurement contact pads, were patterned. Their width W and length L were 70 μm and 210 μm, respectively. Isothermal V–I characteristics were obtained using a DC four-probe method with a voltage resolution of 5 nV, and a stability in the temperature of better than 5 mK. Figure 1 shows $\mathrm{d}R/\mathrm{d}T$ as a function of T. Note that R denotes here the ohmic zero-field resistance. This figure clearly displays a sharp superconducting resistive transition about $T \sim 106.55$ K. An estimate of the width of the transition is obtained from the width, measured at half-maximum, of the $\mathrm{d}R/\mathrm{d}T$ peak. In this way, we find $\Delta T \approx 1.6$ K. Moreover, the resistance as a function of the temperature does not exhibit any 'shoulder' or other anomalies as shown in the inset of the figure. Such electrical characteristics are convincing arguments in favour of the high quality of the Tl-2212 film used in this investigation.

3. Results

Figure 2 shows typical isothermal V–I characteristics obtained for our Tl-2212 thin film. A rough power-law behaviour $V \sim I^{a(T)}$ [28] with a temperature-dependent exponent $a > 3$ is found in the range of lower temperatures, as shown in the inset of the figure above. At higher temperatures, a linear behaviour (ohmic regime) is observed in the lower current density limit. The current crossover I_{cr} between ohmic and non-ohmic regimes is found to decrease rapidly with increasing temperature. We think that the behaviour observed is quite similar to that expected in a BKT transition type. Moreover, we intend to show that the

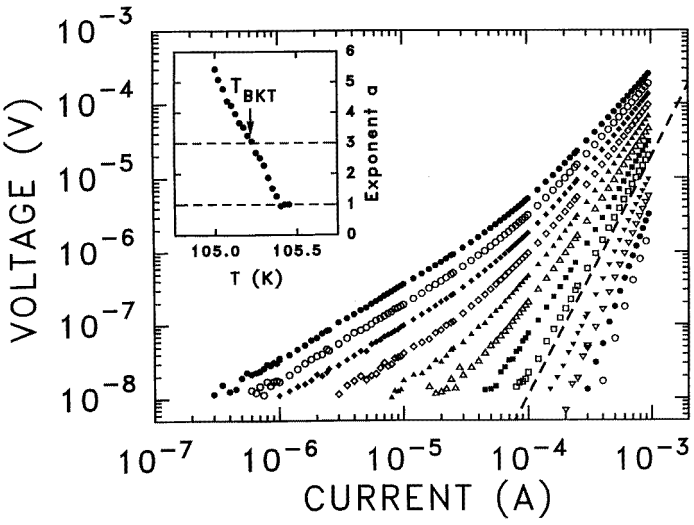

Figure 2. Logarithmic plot of V versus I. From the right to the left the data were obtained at the following temperatures: 105.50 K, 105.050 K, 105.100 K, 105.175 K, 105.225 K, 105.275 K, 105.325 K, 105.375 K, 105.425 K, 105.475 K, 105.525 K and 105.575 K. The broken line is a guide for the eye, its slope is equal to 3. The inset shows the temperature dependence of the exponent $a(T)$ in $V \propto I^{a(T)}$. It is to be noted that $a(T)$ is determined over the range of lower current densities as T lies within the range of higher temperatures.

ohmic regime observed in the low current density limit is due to thermal dissociation at T_{BKT} of large-scale vortex–antivortex fluctuations through the sample inhomogeneities assumed to be arranged two-dimensionally in our thin film. Following this hypothesis the ohmic–non-ohmic crossover, which corresponds to a balance between the thermal effects and the finite current effects, can be described in terms of competition between two characteristic distances. One distance $\xi_I = s(I_c/I)$ is imposed by current effects and the other corresponds to the separation ξ_+ between thermal free vortex excitations. The latter is given on the basis of the BKT theory by $\xi_+ = s \exp[(b/\tau')^{1/2}]$ where b is a non-universal constant of order unity and τ' a reduced temperature given by $\tau' = T'/T_{BKT} - 1$, T' being an effective temperature defined by $T' = TA(T_{BKT})/A(T)$. In this way, the current crossover is expressible by $\xi_{Icr} = \xi_+$, namely

$$I_{cr} = I_c(T) \exp[-(b/\tau')^{1/2}] \tag{1}$$

where $I_c(T) \propto A(T)$; hence $I_c(T) \sim (T_{co} - T)^2$ as discussed above.

On the other hand, LAT have calculated the finite sheet resistance of a junction array arising because dissociated vortices–antivortices are moved by the current and dissipate. It is found that $R_\square = n_v s^2 r_n$ [16] where n_v and r_n are the free vortex density and the normal-state resistance, respectively, of one of the junctions. Above T_{BKT}, as long as thermal effects dominate, $n_v \sim \xi_+^{-2}$, so that the ohmic sheet resistance takes the form

$$R_\square = cr_n \exp[-2(b/\tau')^{1/2}] \tag{2}$$

with c a dimensionless constant of order unity. For an experimental investigation of equations (1) and (2) near T_{BKT}, knowledge of T_{co} is essentially required. Different ways are possible to determine T_{co}; in particular, two methods are well known. One consists of an attempt to fit paraconductivity theories [29, 30] to high-temperature resistive data, and the

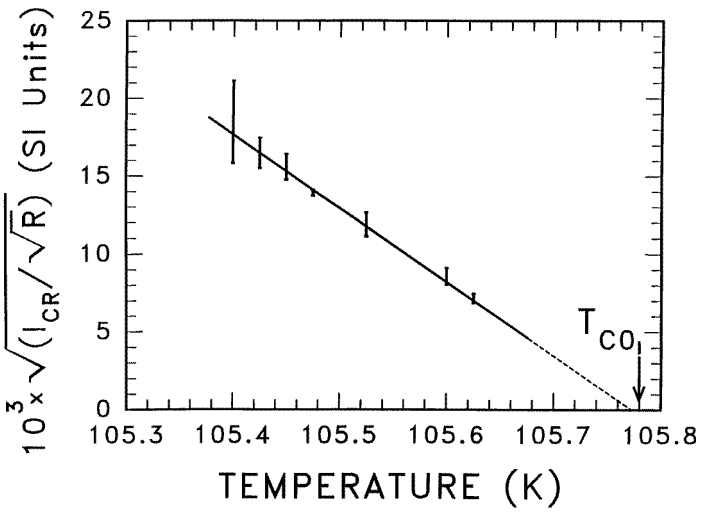

Figure 3. Square root of $I_{cr}/\sqrt{R}$ versus T. I_{cr} denotes the measured current crossover between ohmic and non-ohmic regimes and R the ohmic resistance. The solid line displays a regression which supports $I_c \sim (T_{co} - T)^2$ as shown in the text.

other is an extrapolation of the low-temperature dependence of the exponent $a(T)$ to higher temperatures as long as the Ginzburg–Landau approximation is valid. However, in the case of granular materials, the former is not the most appropriate method. This is because knowledge of the intergrain barrier contribution is necessary for a quantitative description of the excess conductivity which is localized only in the superconducting grains [31]. Here, we propose an unusual way to find T_{co} which appears to be consistent with the latter as will be shown hereafter. Combining equations (1) and (2), it is easy to show that the ratio of I_{cr} to $\sqrt{R_\Box}$ is proportional to I_c so that a measure of $I_{cr}/\sqrt{R_\Box}$ is an additional method for determining both T_{co} and $I_c(T)$. Note that equations (1) and (2) are valid only in the limit of weak τ' so that one expects $I_{cr}/\sqrt{R_\Box} \propto I_c$ to be verified only in any temperature range close to T_{BKT}. We represent in figure 3 the square root of $I_{cr}/\sqrt{R}$ as a function of the temperature. Here, I_{cr} coincides, within the experimental errors, with the threshold current for which the ratio of V/I to R departs from unity, and $\sqrt{R}$ equals the square root of the ohmic resistance. The solid straight line in figure 3 represents the best regression of the temperature dependence $I_c(T) \sim (T_{co} - T)^2$, as predicted above. Moreover, the broken line is an extrapolation of low-temperature data to higher temperatures, giving the value of T_{co}.

Figure 4 shows $\ln R$ against $1/\sqrt{\tau'}$. According to $A(T) \sim (T_{co} - T)^2$, the effective temperature $T' = T(T_{co} - T_{BKT})^2/(T_{co} - T)^2$ has been introduced to calculate the reduced temperature τ', as was defined above, and T_{BKT} is determined in the usual way from $a(T_{BKT}) = 3$ as shown in the inset of figure 2. The straight line in figure 4 represents a least-squares fit of the theoretical equation (2) to the data. Both $R_n = L/Wcr_n$ (L/W being the corrective geometrical factor) and b act as adjustable fitting parameters. The optimum values are $b \approx 5.88$ and $R_n \approx 239$ mΩ. It is to be noted that the former is close to the theoretical value $b \approx 5.14$ found for a square X–Y model [12]. Now, let us return to figure 3 which supports $I_c(T) = I_{co}(1 - T/T_{co})^2$. The intersection of the straight line with the axis of the ordinates gives $(I_{co}/\sqrt{R_n})^{1/2} = 4.92$ in SI units. Then, taking $R_n = 0.239$ and substituting in the preceding expression, we find that $I_{co} \approx 11.83$ Å.

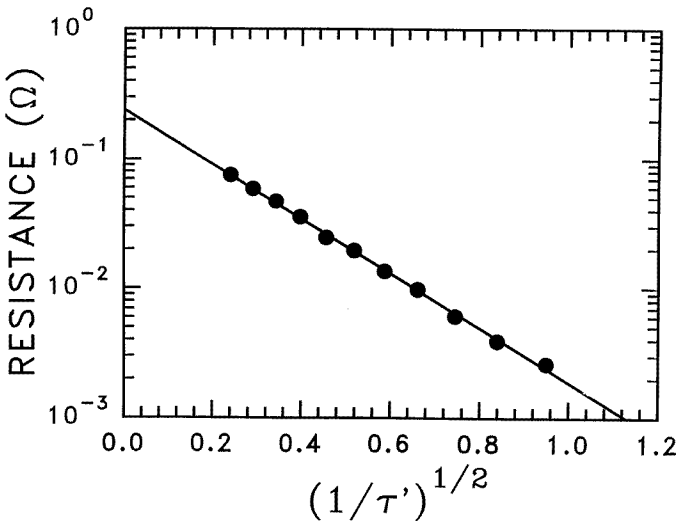

Figure 4. Semilogarithmic plot of R versus $1/\sqrt{\tau'}$. τ' is an effective reduced temperature as shown in the text. The solid line represents an attempt to fit equation (2) to the data.

4. Discussion

A noticeable fact is that the pertinent characteristic current in an array of tunnel junctions is the critical current i_c of a single junction. Here, we shall assume a homogeneous granular thin film. Then, as i is the current through one junction, I and i are related by $I/W = i/s$. Therefore, it can be inferred that $i_c(T) = i_{co}(1 - T/T_{co})^2$. On the other hand, i_{co} is found from the LAT [16] theory which predicts the numerical value

$$i_c(T_{BKT})/T_{BKT} \approx 30 \text{ nA K}^{-1} \tag{3}$$

and hence $i_{co} \approx 117$ mA. Another pertinent parameter is the voltage introduced from the product of r_n and i_{co}, i.e. $V_0 = r_n i_{co}$. In the case of conventional tunnel junctions, V_0 links up with the energy gap 2Δ. For both SIS and SNS tunnel junctions, it is usually expected that $eV_0/2\Delta \approx 1$ where e is the elementary electrical charge. For instance, the well known Ambegaokar–Baratoff [32] expression leads to $eV_0/2\Delta = \pi/4$ for the former type, so that within the weak-coupling BCS limit it is found that $eV_0 = 2.75k_BT_{co}$. Here, under these conditions we find that the dimensionless constant c in equation (2) is approximately equal to unity, in good agreement with the predictions as discussed above.

We shall now concern ourselves with a quantitative evaluation of the consistency of the data with the LAT [16] theory. Both below and above T_{BKT}, there are temperature-dependent length scales which characterize the renormalized interaction for a single vortex–antivortex pair excitation at separation r due to the presence of a background of polarizable vortex pairs with smaller separations. Above T_{BKT}, the characteristic length is ξ_+ as was shown before. Below T_{BKT}, the pertinent length ξ_- is associated with the average separation between bound excitations. ξ_- is given on the basis of the BKT theory by $\xi_- = s\exp(1/(2\pi))(b/|\tau'|)^{1/2}]$ [12, 13]. Note that previous expressions for $\xi_\pm$ are valid only close to T_{BKT}. Both ξ_+ and ξ_- diverge at T_{BKT} so that the BKT fixed point $\pi\kappa_\infty(T_{BKT}) = 2$ is not experimentally observable because of finite size effects. In order to observe the fully renormalized transition, it is necessary that the inequalities $(\xi_-, \xi_+) < \xi_I < W$ be verified where W denotes the greater length accessible in the experiment. Using the equation

$W/s = I_{co}/i_{co}$ with numerical values as determined above, we find that $s \approx 7000$ Å, which accounts for a realistic effective grain size in our granular thin film. By doing this we *really* obtain $\xi_{\pm}$ and ξ_I. In figure 5 we have plotted $\ln(\xi_{\pm}/s)$ and $\ln(\xi_I/s)$ as functions of the temperature. ξ_+ and ξ_- are represented by the two dotted curves, respectively, and the typical distances probed by the current in our experiment are shown by the solid curves. The horizontal chain line represents W. Above T_{BKT}, figure 5 clearly shows that the condition $\xi_+ < \xi_I$ holds only within the range of weak currents for $T > 105.375$ K. Likewise, below T_{BKT} we have difficulty in achieving $\xi_- < \xi_I$. Thus, in our experiment, because ξ_I is the shortest characteristic length over almost the entire region of interest, the measured quantities are partially renormalized. This means that the magnitudes of external current determine the length scale over which the renormalized interaction is probed. Therefore, it is dependent on either ξ_I or $\ell_I \equiv \ln(\xi_I/s) = \ln(I_c/I)$.

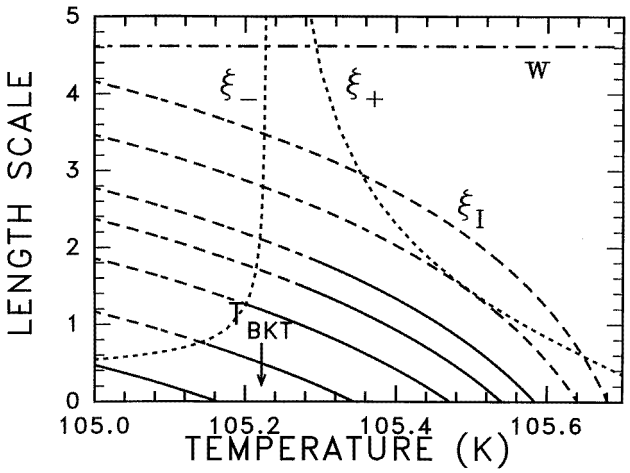

Figure 5. Natural logarithms of ξ_-, ξ_+ and ξ_I (in units of s with $s \sim 7000$ Å) versus T. The dotted lines show ξ_- and ξ_+ which diverge at T_{BKT}. The horizontal chain line accounts for finite size effects. Both the solid and the broken curves display length scales associated with current; from the right to the left $I = 10$ μA, 20 μA, 40 μA, 60 μA, 100 μA, 200 μA and 400 μA. The solid curves exhibit typical length scales over which the interaction is probed by the current in the experiment.

The density of free vortices can be expressed in terms of the pair excitation probability $y(\ell)$ by $n_v \approx s^{-2}\exp(-2\ell)y(\ell)$ where ℓ is a convenient dimensionless quantity defined as $\ell \equiv \ln(r/s)$; hence $V/I \propto \exp(-2\ell_I)y(\ell_I)$ within the regimes for which the conditions $\xi_I \ll (\xi_-, \xi_+) < W$ hold [24]. Following KEG, $V/I \propto \exp(-2\ell_I)y(\ell_I)$ together with the Kosterlitz scaling equation $\mathrm{d}y/\mathrm{d}\ell_I = (2 - \pi\kappa_{\ell_I})y(\ell_I)$ give [24]

$$\mathrm{d}[\ln(V/I)]/\mathrm{d}[\ln I] = \pi\kappa_{\ell_I}(T). \tag{4}$$

For the range of currents in our experiment, ℓ_I lies between 0 and 3 as shown in figure 5, which does not allow us to investigate the large length scale limit. In particular, the well known universal Nelson–Kosterlitz [33] jump in the fully renormalized stiffness constant $\pi\kappa_\infty$ from 2 to 0 at T_{BKT} is blurred as shown in the inset of figure 2. However, note that exponent $a(T)$, as was defined before, cannot show evidence of the spatial renormalization of the vortex interaction. Assuming that equation (4) still holds as ℓ_I equals zero, i.e. $I = I_c$, we represent in figure 6 the experimental values of $\pi\kappa_0$ obtained by applying

equation (4). A significant fact is the weak variation rate of $\pi\kappa_0(T)$ in comparison with the exponent $a(T)$ for higher temperatures. It can be clearly seen that $\pi\kappa_0(T)$ undergoes a variation throughout the temperature range which rejects a linear form. The solid curve in figure 6 represents a smoothing to the data from which we obtain that $\pi\kappa_0(T)$ almost vanishes at T_{co}, in good agreement with the usual method to determine T_{co} as was shown above. Another way to find $\pi\kappa_0$ consists in applying the relation $\pi\kappa_0 = A/2k_BT$ in which we take an expression for the vortex interaction constant as $A(T) = \phi_0 i_c(T)$ [17] where $\phi_0 = h/2e$ is the elementary quantum flux. In this way, the solid curve in figure 6 is in very good agreement with the expected behaviour of $\pi\kappa_0$ with respect to temperature when $i_c(T) = i_{co}(1 - T/T_{co})^2$ fulfills the theoretical value as was shown in equation (3). Here, it should be kept in mind that two *independent* ways have been used to reach $\pi\kappa_0$. One method investigates both the weak- and the intermediate-current limits above T_{BKT} with corresponding inequalities for the characteristic distances $s < \xi_+ \leqslant \xi_I < W$, and the other consists in probing the strong current limit in order to make $\xi_I = s$ about T_{BKT}. We find a good consistency between these, which shows evidence of a BKT-like behaviour with a vortex interaction constant $A(T) \sim (T_{co} - T)^2$ as discussed above. On the other hand, an estimate of the effective vortex dielectric constant at T_{BKT} can be obtained from $\epsilon_c = \pi\kappa_0(T_{BKT})/2$. We find the value $\epsilon_c \approx 1.1$ which shows a weak renormalization of the vortex interaction in agreement with the expected value $\epsilon_c = 1.176$ for a square X–Y model [12]. Under these conditions, $a(T_{BKT}) = 3$ gives a close approximation to the BKT fixed point as was assumed above.

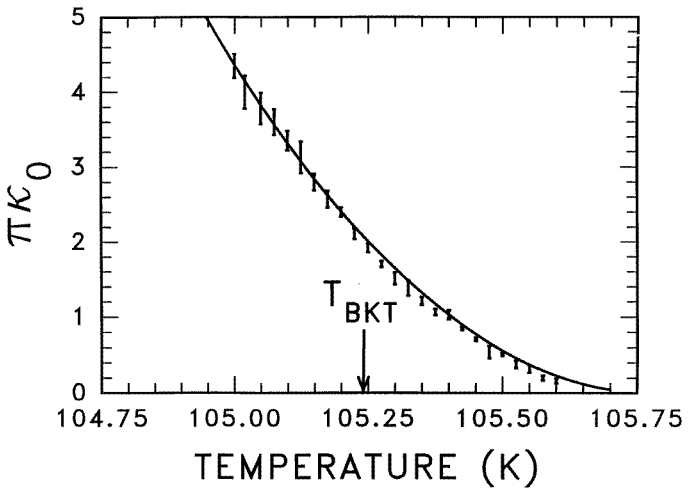

Figure 6. Unrenormalized stiffness constant versus temperature. The short vertical lines with bars and the solid curve are obtained from two independent ways respectively. One way consists in applying equation (4) as ℓ_I equals zero, i.e. $I = I_c(T)$, and the other amounts to using $\pi\kappa_0 = A/2k_BT$ where $A(T) = \phi_0 i_c(T)$ with $i_c(T) \sim (T_{co} - T)^2$ verifying equation (3).

A more quantitative evaluation of the consistency of the data with the LAT [16] theory can be obtained in using the analytic solutions of the Kosterlitz scaling equations [12, 34] as was first pointed out by KEG [24]. As may be seen by setting $\ell_I = \ln(I_c/I)$ in $V/I \propto \exp(-2\ell_I)y(\ell_I)$, a measure of the ratio of V to I^3 allows us to investigate the pair excitation probability as long as current effects are dominating. Therefore, it is useful to

introduce an expression as was shown elsewhere [24]:

$$y(\ell_I) = c'[V/V_c(T)]/[I/I_c(T)]^3 \tag{5}$$

in which the scaling voltage $V_c(T) = R_n I_c(T)$ and c' is an adjustable dimensionless constant. Applying equation (5), we have plotted, in figure 7, y as a function of $\ell_I = \ln(I_c/I)$ about T_{BKT}. The data clearly show that I–V curves indeed exhibit a curvature depending on the current. The solid lines display an attempt to fit the analytic solutions of the Kosterlitz scaling equations [12, 34] to our data. It is useful to keep in the mind that Kosterlitz equations which require $y(\ell) \ll 1$ to be valid have analytic solutions only when the quantity $x(\ell) = 2/\pi\kappa_\ell - 1$ is much less than unity, i.e. $\pi\kappa_\ell \approx 2$. Therefore, we have carried out the fit about T_{BKT} as long as the inequality $|x(0)| < 0.3$ holds. Indeed, figure 7 shows that the theoretical curves and experimental data quantitatively agree. Here, note that c' acts as the one and only fitting parameter in equation 5. It is chosen in such a way that the critical starting conditions are related to one another through the critical trajectory $2\pi y(0) = -x(0)$ in agreement with the renormalized Kosterlitz–Thouless phase transition theory. In this way, we find that $c' \approx 1.24$ which is a reasonable value of order unity. Finally, this analysis shows evidence of a BKT-like behaviour with the length scale of the renormalization determined by the current.

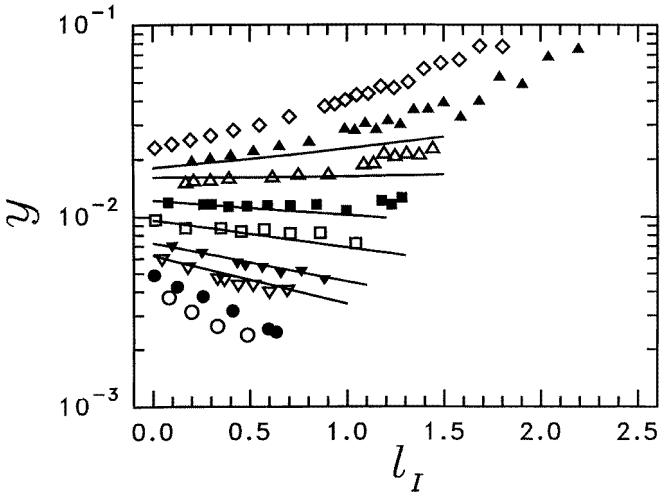

Figure 7. Plots of y versus $\ln(I_c/I)$. Data are obtained by applying equation (5). From the top to the bottom, $\tau' = 0.319$, $\tau' = 0.191$, $\tau' = 0.081$, $\tau' = -0.014$, $\tau' = -0.098$, $\tau' = -0.172$, $\tau' = -0.236$, $\tau' = -0.293$ and $\tau' = -0.345$. The solid lines display an attempt to fit the analytic solutions of the Kosterlitz scaling equations to the data.

As a final point we now discuss the fluctuation conductivity above T_{co}. According to theoretical predictions, paraconductivity in layered compounds is given by the so-called Lawrence–Doniach [30] expression:

$$\sigma_{LD} = g/(d^2\epsilon^2 + 4\xi_\perp^2(0)\epsilon)^{1/2} \tag{6}$$

where $\epsilon = (T - T_{co})/T_{co}$, $g = e^2/16\hbar = 1.52 \times 10^{-5}\ \Omega^{-1}$ is a universal conductance, $\xi_\perp(0)$ is the perpendicular coherence length at $T = 0$, and d is the distance between superconducting layers. Consistently with the features investigated above, we assume here that paraconductivity is localized in the grains and does not affect the barrier

resistivity ρ_b. Hence it follows that the total resistivity of the sample can be written as $\rho = \rho_b + 1/(\sigma_{GN} + \sigma_{LD})$ where $\rho_{GN} = 1/\sigma_{GN}$ denotes the normal resistivity of the grains. In this model fist proposed by Rosenblatt *et al* [31], the experimentally measured quantity is the difference $\delta\rho$, due to the intragranular fluctuation conductivity, between the experimental resistivity $\rho(T)$ and the normal resistivity $\rho_N(T) = \rho_{GN}(T) + \rho_b(T)$. An expression is easily deduced for $\delta\rho$ as $\rho_N - \rho = \sigma_{LD}\rho_{GN}^2/(1 + \sigma_{LD}\rho_{GN})$ from which we obtain $\sigma_{LD}(T)$, if once both $\rho_N(T)$ and $\rho_b(T)$ are known. For this purpose, we estimate $\rho_N(T)$ by extrapolating the linear best fit to the experimental $\rho(T)$ at $T > 250$ K, as shown in the inset of figure 1, and approximate ρ_b to $\rho(T_{co})$ which presupposes that $\rho_b(T)$ is slowly varying with the temperature. Figure 8 shows $g^2\sigma_{LD}^{-2}\epsilon^{-1}$ as a function of ϵ. The solid straight line displays an attempt to fit the theoretical equation (6) to the data. Note that we introduce here only two fitting parameters. One is the intersection of the straight line with the axis of the ordinates that gives the quantity $4\xi_\perp^2(0)$, and the other is the slope of the line from which we obtain d^2. The inset of figure 8 is an enlargement of the figure in the weak reduced-temperature region. It really does show excellent agreement between the theoretical line and data with realistic values for fitting parameters, as expected in the Tl-2212 compound. We find $d \approx 17.7$ Å which is a value close to the half c-axis parameter, and $\xi_\perp(0) \approx 0$. In another redundant way, the solid line in figure 1 fits theoretical predictions, as proposed above, for the experimental $\mathrm{d}R/\mathrm{d}T$. It may then be verified that we *quantitatively* explain, over a very wide temperature range, the 'rounding' of the resistive transition in terms of fluctuation conductivity, as predicted in high-T_c cuprates.

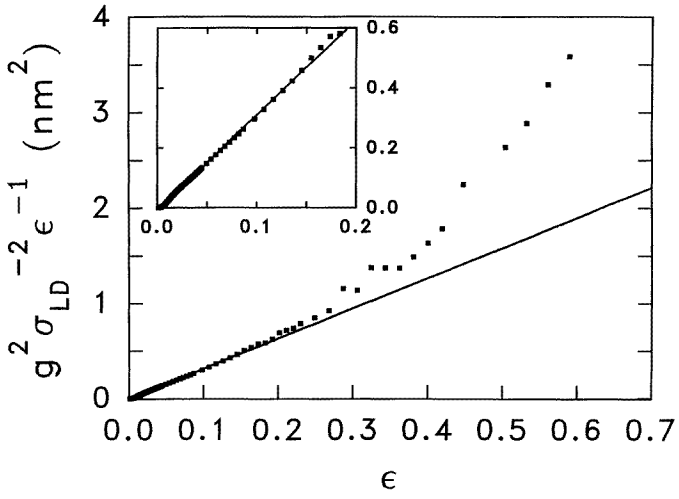

Figure 8. Plot of $g^2\sigma_{LD}^{-2}\epsilon^{-1}$ versus $\epsilon = (T - T_{co})/T_{co}$. The straight line corresponding to the best fit to the data allows the determination of d and $\xi_\perp(0)$.

5. Conclusion

In summary, the present paper reports electrical transport properties near the superconducting critical temperature in a Tl-2212 granular thin film in a zero magnetic field. We find experimental support for a BKT-type phase transition. Using an unusual way to determine the vortex–antivortex interaction constant, we find that $A(T) \sim (T_{co} - T)^2$. This behaviour

cannot account for 2D vortex pair excitations within the superconducting CuO_2 layers. Here we succeed in explaining experimental data which support the view that some Tl-2212 thin films can be described as 2D arrays of weakly coupled superconducting grains. By doing this, we show that data support the LAT [16] model. In particular, a quantitative agreement with the approximate BKT fixed point given by $i_c(T_{BKT})/T_{BKT} \approx 30$ nA K^{-1} is obtained in our experiment. Under these conditions, $A(T) \sim (T_{co} - T)^2$ provides support for a strongly depressed superconducting order parameter at the boundaries, as predicted elsewhere [19, 20]. Using a method first proposed by KEG [24], we investigate in some detail the spatial renormalization of the vortex interaction over length scales imposed by the current. In this way, good agreement with the renormalized BKT theory is found. Finally, the 'rounding' of the resistive transition at $T > T_{co}$ is quantitatively explained by Gaussian fluctuations of the order parameter amplitude, if once the role of the granularity is taken into account.

References

[1] Sugahara M, Kojima M, Yoshikawa N, Akeyoshi T and Haneji N 1987 *Phys. Lett.* **125A** 429
[2] Stamp P C E, Forro L and Ayache C 1988 *Phys. Rev.* B **38** 2847
[3] Martin S, Fiory AT, Fleming R M, Espinosa G P and Cooper A S 1989 *Phys. Rev. Lett.* **62** 677
[4] Yeh N C and Tsuei C C 1989 *Phys. Rev.* B **39** 9708
[5] Artemenko S N, Gorlova I G and Latyshev Yu I 1989 *Pis'ma Zh. Eksp. Teor. Fiz.* **49** 566 (Engl. Transl. 1989 *JEPT Lett.* **49** 654)
[6] Kim D H, Goldman A M, Kang J H and Kampwirth R T 1989 *Phys. Rev.* B **40** 8834
[7] Ying Q Y and Kwok H S 1990 *Phys. Rev.* B **42** 2242
[8] Paracchini C, Romano L and Francesio L 1991 *Physica* C **175** 324
[9] Pradhan A K, Hazell S J, Hodby J W, Chen C, Hu Y and Wanklyn B M 1993 *Phys. Rev.* B **47** 11 374
[10] Livanov D V, Balestrino G and Montuori M 1994 *Physica* C **226** 320
[11] Berezinskii V L 1970 *Zh. Eksp. Teor. Fiz.* **59** 907 (Engl. Transl. 1971 *Sov. Phys.–JETP* **32** 493)
[12] Kosterlitz J M and Thouless D J 1973 *J. Phys. C: Solid State Phys.* **6** 1181
[13] Mooij J E 1984 *Percolation, Localization and Superconductivity (NATO ASI Series B: Physics 109)* ed A M Goldman and S A Wolf (New York: Plenum) p 325
[14] Hikami S and Tsuneto T 1980 *Prog. Theor. Phys.* **63** 387
[15] Paracchini C and Romano L 1993 *Physica* C **207** 143
[16] Lobb C J, Abraham D W and Tinkham M 1983 *Phys. Rev.* B **27** 150
[17] Here, we consider tunnel junction arrays in the weak-coupling limit, where the relation between the superconducting phase difference on two neighbouring nodes and the pair current flowing out between them is sine shaped.
[18] de Gennes P G 1989 *Superconductivity of Metals and Alloys* (Reading, MA: Addison-Wesley) p 232
[19] Deutscher G and Müller K A 1987 *Phys. Rev. Lett.* **59** 1745
[20] Deutscher G 1988 *Physica* C **153–5** 15
[21] Buzdin A and Feinberg D 1990 *J. Physique* **51** 1971
[22] Clem J R 1991 *Phys. Rev.* B **43** 7837
[23] Martynovich A Yu 1993 *Pis'ma Zh. Eksp. Teor. Fiz.* **58** 804 (Engl. Transl. 1993 *JETP Lett.* **58** 750)
[24] Kadin A M, Epstein K and Goldman A M 1983 *Phys. Rev.* B **27** 6691
[25] Coudrier L, Mercey B and Murray H 1993 *Supercond. Sci. Technol.* **6** 119
[26] Gasser C, Taffin A, Mercey B, Studer F and Murray H 1996 *J. Solid State Chem.* **121** 262
[27] Lee W Y, Lee Y V, Salem J, Huang T C, Savoy R, Bullok D C and Parkin S S P 1988 *Appl. Phys. Lett.* **53** 329
[28] In fact, the $V–I$ curves on the log–log plot in figure 2 are not all perfectly straight within the range of the lower temperatures as will be shown below.
[29] Aslamazov L G and Larkin A I 1968 *Fiz. Tverd. Tela* **10** 1104 (Engl. Transl. 1968 *Sov. Phys. Solid State* **10** 875)
[30] Lawrence W E and Doniach S 1971 *Proc. 12th Int. Conf. on Low Temperature Physics (Kyoto, 1970)* ed E Kanda (Tokyo: Keigaku) p 361
[31] Rosenblatt J, Raboutou A, Peyral P and Lebeau C 1990 *Rev. Phys. Appl.* **25** 73

[32] Ambegaokar V and Baratoff A 1963 *Phys. Rev. Lett.* **10** 486; 1963 *Phys. Rev. Lett.* **11** 104
[33] Nelson D R and Kosterlitz J M 1977 *Phys. Rev. Lett.* **39** 1201
[34] Ambegaokar V, Halperin B I, Nelson D R and Siggia E D 1980 *Phys. Rev.* B **21** 1806